Random sequential adsorption on a triangular lattice

Lj. Budinski-Petković and U. Kozmidis-Luburić

Faculty of Engineering, Trg D. Obradovića 6, 21000 Novi Sad, Yugoslavia

(Received 19 February 1997; revised manuscript received 6 June 1997)

Random sequential adsorption of objects of various shapes on a planar triangular lattice is studied by Monte Carlo simulation. Various shapes are made by self-avoiding random walks on the lattice. At the late stage of deposition, the approach to the jamming coverage is exponential for all shapes and of the same form as for the square lattice. Jamming configurations consist of clusters of blocked sites and domains of parallel deposited objects. The jamming coverage decays exponentially with the size s of the deposited objects. For the deposition of mixtures the jamming coverage increases with the number of components in the mixture. [S1063-651X(97)09411-7]

PACS number(s): 61.43.−j

I. INTRODUCTION

A number of processes in physics, chemistry, and biology, where events occur essentially irreversibly on the time scales of interest, may be modeled by random sequential adsorption (RSA) on a lattice. RSA, or irreversible deposition, is a process in which objects of a specified shape are randomly and sequentially adsorbed on a substrate.

In real systems one needs to take into account the interaction between the bulk particles and the surface and also the interaction between the adsorbed and the bulk particles. We shall focus our attention on the case in which the particle-surface interaction disallows desorption from or diffusion on the surface and its range is small compared to the size of the particles. We shall also assume that the forces among the adsorbing particles are repulsive, so they allow formation of only one layer. Since the diffusion of adsorbed objects is not allowed, once an object is placed it affects the geometry of all later placements, even though each placement happens completely randomly. Thus the dominant effect in RSA is the blocking of the available substrate area and the limiting (''jamming'') coverage $\theta(\infty)$ is less than in close packing. The kinetic properties of a deposition process are described by the time evolution of the coverage $\theta(t)$, which is the fraction of the substrate area occupied by the adsorbed particles. For a review of RSA models, see [1].

Experimentally, RSA has been observed, for example, in oxidation of one-dimensional polymer chains [2], formation of polymer brush films [3], adhesion of colloidal particles on solid substrates [4], adsorption of proteins at phospholipid bilayers that are the natural surface for adsorption of proteins in living cells [5], particles in biological membranes [6], and spatial patterns in ecological systems [7].

In one dimension most problems have been solved analytically [8–10]. The placing of an object on a line divides the line into two independent systems that can be treated separately. It is this property that has made analytic progress possible and it does not exist for two-dimensional lattices. Theoretical studies of RSA also include series expansions [11–13] and Monte Carlo simulations [14–19].

Depending on the system of interest, the substrate can be continuum or discrete and RSA models can differ in substrate dimensionality. For lattice RSA models, the approach to the jamming coverage is exponential [16–18]:

$$\theta(t) = \theta(\infty) - A e^{-t/\sigma}, \qquad (1)$$

where A and σ are parameters that depend on the shape and orientational freedom of depositing objects. In a Monte Carlo study [16] of the deposition of line segments on a square lattice, it was found that A depends on the line length l ($A \sim 1/l$), but σ is independent of l with a numerical value $\sigma \simeq 0.5$. The jamming coverage decreases exponentially with the size of depositing objects for small object sizes (measured in lattice spacing) [17].

Much attention has been paid to the RSA on square lattices, but there are only a few studies of RSA on other types of lattices such as triangular or hexagonal lattices [1,20].
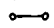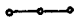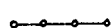
II. KINETICS OF IRREVERSIBLE DEPOSITION ON A TRIANGULAR LATTICE

In the present work we study irreversible deposition of objects of various shapes on a triangular lattice by Monte Carlo simulations. The depositing objects are formed by self-avoiding random walks on the lattice. For a small number of steps it is easy to find all the shapes that may have a different long-time behavior of $\theta(t)$ and different jamming coverages $\theta(\infty)$. In order to make a systematic approach to this problem, we performed numerical simulations for all suc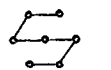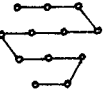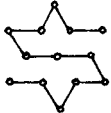h shapes of length, $l = 1$, 2, and 3. The results of these simulations are shown in Table I. On a triangular lattice we can form shapes with a symmetry axis of first, second, third, and sixth order. In order to have at least two representative objects for each order of symmetry, we performed the simulations for three more objects, one with a symmetry axis of third order and two with symmetry axes of sixth order, and these results are also given in Table I.

The Monte Carlo simulations are performed on a triangular lattice of size $L = 128$. Periodic boundary conditions are used in all directions and objects are not allowed to overlap.

At each deposition attempt we randomly select a lattice site. If the selected site is unoccupied, we try to deposit the object, i.e., we fix the beginning of the walk that makes the shape at this site and try to place it in any of the six possible orientations. If all successive l sites are unoccupied we oc-
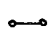
TABLE I. Parameters σ and A and jamming coverages $\theta(\infty)$ for various shapes on a triangular lattice. Plots of $\theta(\infty)$ vs s are shown in Fig. 2, as marked in the last column.

shape		σ	A	$\theta(\infty)$	
$\ell = 1$	o—o	0,548	1,168	0,9243	(1)
$\ell = 2$	o—o—o	0,562	1,016	0,8456	
		1,067	0,287	0,8386	(3)
		0,451	0,803	0,8139	(2)
$\ell = 3$	o—o—o—o	0,575	0,894	0,7960	
		1,091	0,327	0,7699	(5)
		1,059	0,303	0,7712	(8)
		0,594	1,030	0,7461	(6)
		1,085	0,387	0,7677	(7)
		1,087	0,353	0,7232	(9)
		0,559	0,495	0,7682	(4)
		1,054	0,290	0,7770	(10)
		1,069	0,267	0,7773	(11)
$\ell = 6$		0,337	0,278	0,6847	(12)
$\ell = 11$		0,460	0,944	0,6545	
$\ell = 12$		0,328	0,297	0,6132	

TABLE II. Parameters θ_0, θ_1, and r for various shapes. Simulations are performed for these basic shapes of sizes $s \leq 10$ in lattice spacing. Plots of $\theta(\infty)$ vs s are shown in Fig. 2, as marked in the last column.

basic shape	θ_0	θ_1	r	
o—o	0,6741	0,3298	3,1405	(1)
	0,6086	0,3882	1,6621	(2)
	0,5038	0,4966	3,7284	(3)
	0,6001	0,3980	1,8272	(4)
	0,4941	0,5052	4,1862	(5)
	0,4925	0,5063	3,7163	(6)
	0,4822	0,5161	3,4796	(7)
	0,4465	0.5508	3,9779	(8)
	0,3287	0,6708	3,7873	(9)
	0,3414	0,6602	4,6614	(10)
	0,4419	0,5564	4,0734	(11)
	0,5887	0,4109	1,4104	(12)

cupy these $l+1$ sites and deposit the segment. If the attempt fails, we randomly choose another orientation and so on, until a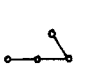ll six possibilities are examined. In the case that the object cannot be placed in any of the six directions, this site is denoted as inaccessible. During the simulation we record the number of all inaccessible sites in the lattice. These include the occupied sites and the sites that are unoccupied but cannot be the beginning of the walk. If we select an inaccessible site, we do not attempt to deposit the object but increase the time by one unit. The jamming limit is reached when the number of inaccessible sites is equal to the total number of sites in the lattice. The time is counted by the number of attempts to select a lattice site and scaled by the total number of lattice sites. The data are averaged over 100 independent runs for each shape.

For all the shapes from Table I plots of $\ln[\theta(\infty) - \theta(t)]$ vs t are straight lines for the late stages of deposition. This suggests that the approach to the jamming limit in the case of a

triangular lattice is also exponential and of the form (1), the same as in the case of a square lattice, with parameters σ, A, and $\theta(\infty)$, which depend on the shape of a deposited object.

The parameters σ and A depend also on the orientational freedom of deposited objects and they are very sensitive to the rules of deposition. The values of the rate σ are determined from the slope of the lines and for the described model they depend mostly on the order of symmetry of the shape. According to σ, all the shapes from Table I can be divided into four groups: (i) shapes with a symmetry axis of first order with $\sigma \approx 1.1$, (ii) shapes with a symmetry axis of second order with $\sigma \approx 0.57$, (iii) shapes with a symmetry axis of third order with $\sigma \approx 0.46$, and (iv) shapes with a symmetry axis of sixth order with $\sigma \approx 0.33$. The shapes with a higher order of symmetry have lower values of σ, which means that they approach their jamming limit more rapidly.

Simulations are also performed for various sizes of the basic shapes shown in the first column of Table II. For each given basic shape, numerical results are obtained for sizes ≤ 10 in lattice spacing. These objects can be considered as small and at the same time the finite-size effects can be neglected [16]. The size s is taken as the greatest dimension of the object, i.e., as the greatest projection of the walk that makes the object on one of the six directions. Thus the dimension of a dot is $s = 0$, the dimension of a one-step walk is

a)

b)
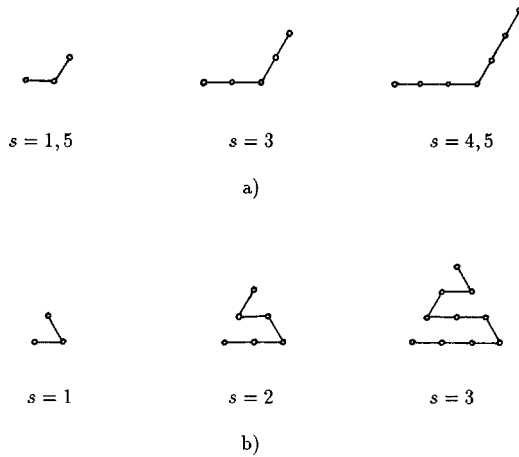
FIG. 1. Illustration of the construction of the objects larger than the basic ones: (a) the basic shape marked in the tables with (3) and the objects obtained by repeating each step of this object two and three times and (b) triangles of size 1–3 in lattice spacing.
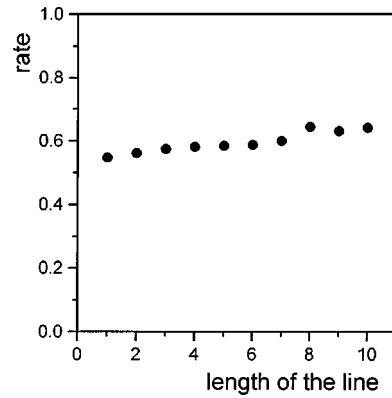
FIG. 2. Rate σ vs the length of the lines (in lattice spacing).
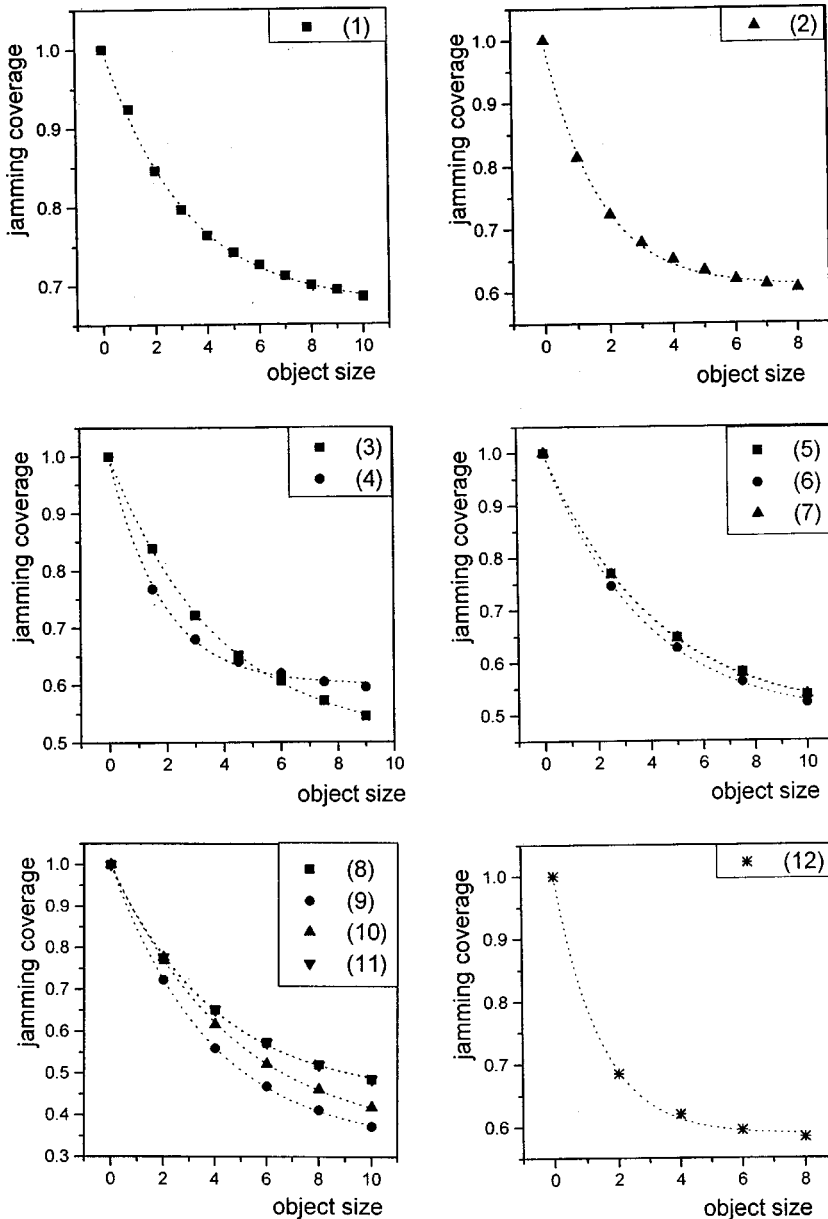
FIG. 3. Dependence of $\theta(\infty)$ on the size of depositing objects (in lattice spacing) for the basic shapes from Table II, marked with corresponding numbers. The dotted lines represent the exponential fit of the form $\theta(\infty) = \theta_0 + \theta_1 e^{-s/r}$.

FIG. 4. Jamming coverages for deposition of line segments on a triangular (triangles) and square (squares) lattice vs the length of the lines (in lattice spacing).

$s = 1$, and for example, the dimension of the object marked in the tables with (3) is $s = 1.5$ in lattice spacing. Objects of various sizes are made by repeating each step of a basic shape the same number of times. Exception is made for triangles and hexagons, marked in the tables with (2) and (12), respectively, where larger objects also occupy all comprised sites. The construction of larger objects is illustrated in Fig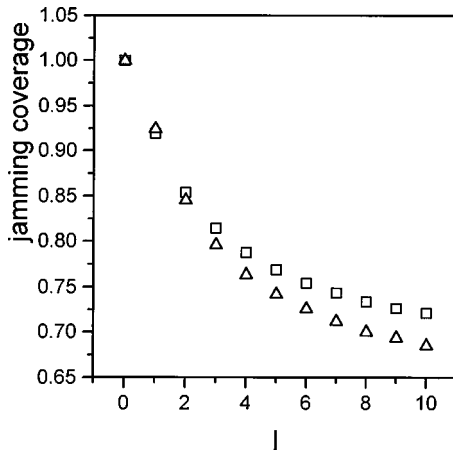. 1. In Fig. 1(a) the basic shape marked in the tables with (3) is shown together with the objects obtained by repeating each step of this object two and three times and their sizes are 1.5, 3, and 4.5 respectively. Triangles of size 1–3 are shown in Fig. 1(b). The way in which the sites are connected is irrelevant because it is the arrangement of the occupied sites that matters.

When a dimension of an object increases, a slight increase of σ with respect to the value for the basic shape was found. This dependence is shown in Fig. 2 for straight lines and it is similar for all the shapes. This kind of dependence might be a consequence of the rules of deposition we used, together with the orientational freedom of depositing objects, i.e., in the case of a square lattice σ does not depend on the size of depositing objects [16,17], suggesting that this difference is due to the number of possible orientations on a square and a triangular lattice.

On the other hand, the parameter A decreases with the object size for the same type of shape. This kind of behavior was also observed for the square lattice [16,17].

III. JAMMING COVERAGES AND JAMMING CONFIGURATIONS ON A TRIANGULAR LATTICE

Jamming coverage $\theta(\infty)$ depends on the shape of the object and on its dimension. Qualitatively, we could say that it depends on the local geometry of the shape, i.e., on the probability that the neighboring sites of an adsorbed object would be blocked by another adsorbed object. For a fixed l, $\theta(\infty)$ has the highest values for straight lines.

For the same type of shape the jamming coverage decreases when the size of the object increases. The plots of $\theta(\infty)$ vs s for the basic shapes from Table II are shown in Fig. 3 and marked with corresponding numbers. The dotted lines represent the exponential fit of the form
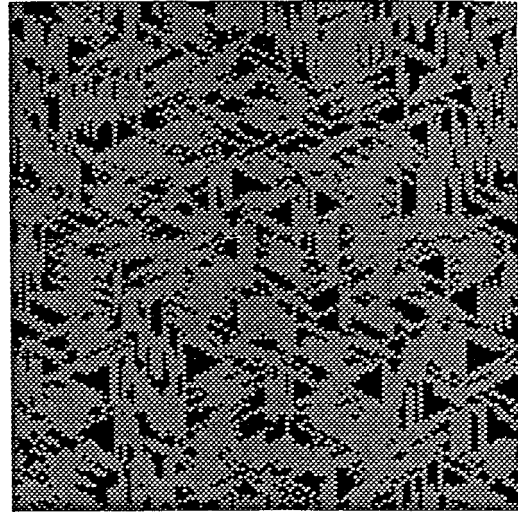

FIG. 5. Typical jamming configuration on a triangular lattice for straight lines of length $l = 10$ (in lattice spacing). Blocked regions are black and occupied sites are shown in white.

$$\theta(\infty) = \theta_0 + \theta_1 e^{-s/r}, \quad (2)$$

where θ_0, θ_1, and r are parameters that depend on the object shape and are given in Table II for each basic shape. From Fig. 3 we can see that the couples of shapes marked with (5) and (7) and with (8) and (11) show a similar behavior of jamming coverage with the object size, suggesting that it is rather irrelevant which end of the walk we fix at the chosen site.

Jamming coverages for the deposition of straight lines on a triangular and a square lattice are shown together vs the length of the lines in Fig. 4. We can see that the jamming coverages have greater values on the square lattice (except for one-step lines). This difference is due to the orientational freedom of depositing lines: On a triangular lattice there is a greater number of possible orientations and an enhanced probability for blocking of lattice sites. This effect is more prominent for longer lines.

A typical jamming configuration for the deposition of line segments of length $l = 10$ is shown in Fig. 5. At very early times, deposited lines do not "feel" the presence of the others and are adsorbed in any of the six orientations with the same probability. However, lines deposited in the late stages of deposition must deposit parallel to the already deposited ones in order to avoid an intersection. The jamming configuration consists of domains of parallel lines and of clusters of blocked sites. If the depositing objects are not straight lines, there are also clusters of blocked sites in the jamming configurations, but their sizes are smaller. Sizes of these clusters are proportional to the size of depositing objects.

IV. JAMMING COVERAGES FOR DEPOSITION OF MIXTURES OF LINE SEGMENTS

Jamming coverages for the deposition of mixtures of straight lines of various lengths on a triangular lattice are also determined numerically. Simulations are performed for two-component, three-component, and up to eight-component mixtures. In the case of the two-component mix-
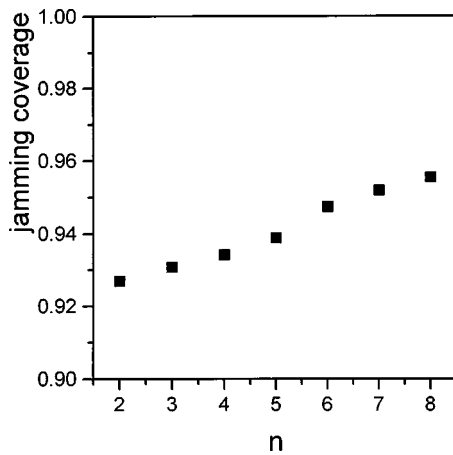
FIG. 6. Dependence of $\theta(\infty)$ on the number of components (line segments of various lengths) in the mixture.

ture lines of length $l=1$ and 2 are adsorbed with equal probability. The three-component mixture is made by adding a line segment of length $l=3$ and so on. Generally, an n-component mixture contains lines of length $l=1,2,...,n$ and all of them are adsorbed with equal probability. A lattice site is denoted as inaccessible if it is occupied or it cannot be the beginning of either of the components, i.e., a line segment of length $l=1$ cannot be placed with one end in that site. The data are averaged over 100 independent runs for each mixture.

The dependence of $\theta(\infty)$ on the number of components in the mixture n is shown in Fig. 6. We can see that the jamming coverage increases with n, in spite of the fact that the number of components is always increased by adding a line segment of a greater length.

V. CONCLUSION

We have studied the single-layer deposition of objects of various shapes on a triangular lattice. The shapes are made by self-avoiding random walks on the lattice. The approach to the jamming limit is exponential for all the shapes with the rate σ dependent mostly on the order of symmetry of the shape. The shapes of higher order of symmetry have lower values of σ, i.e., they approach their jamming limit more rapidly.

The jamming coverage $\theta(\infty)$ depends on the local geometry of the shape, i.e., on the shape and size of the adsorbing object. For a fixed length of the walk that makes the shape, $\theta(\infty)$ has the highest values for straight lines, which have the lowest probability for blocking their neighboring sites. The jamming coverage decays exponentially with the size of the object for small object sizes. If we compare results for RSA of straight lines on a square and a triangular lattice, this decay is more rapid for a triangular lattice.

Jamming patterns consist of clusters of blocked sites and of domains of parallel deposited objects. The sizes of clusters of blocked sites are proportional to the size of deposited objects and the sizes of domains of parallel deposited objects are greater for elongated shapes.

The jamming coverage for the deposition of mixtures increases with the number of components in the mixture. This effect is ''stronger'' than the decrease of the jamming coverage with the maximal length of the components that make the mixture.

[1] J. W. Evans, Rev. Mod. Phys. **65**, 1281 (1993).
[2] J. J. Gonzalez, P. C. Hemmer, and J. S. Hoye, Chem. Phys. **3**, 228 (1974).
[3] A. Karim, V. V. Tsukruk, J. F. Douglas, S. K. Satija, L. J. Fetters, D. H. Reneker, and M. D. Foster, J. Phys. II **5**, 1441 (1995).
[4] N. Kallay, M. Tomić, B. Biskup, I. Kunjašić, and E. Matijević, Colloids Surface **29**, 185 (1987).
[5] J. J. Ramsden, G. I. Bachmanova, and A. I. Archakov, Phys. Rev. E **50**, 5072 (1994).
[6] L. Finegold and J. T. Donnell, Nature (London) **278**, 443 (1979).
[7] M. Hasegawa and M. Tanemura, in *Recent Developments in Statistical Interference and Data Analysis*, edited by K. Matusita (North-Holland, Amsterdam, 1980).
[8] R. Swendsen, Phys. Rev. A **24**, 504 (1981).
[9] E. Ben-Naim and P. L. Krapivsky, J. Phys. A **27**, 3575 (1994).
[10] N. O. Wolf, J. W. Evans, and D. K. Hoffman, J. Math. Phys. (N.Y.) **25**, 2519 (1984).
[11] J. Evans and R. S. Nord, J. Stat. Phys. **38**, 681 (1985).
[12] M. Nakamura, Phys. Rev. A **36**, 2384 (1987).
[13] P. Schaaf, J. Talbot, H. M. Rabeony, and H. Reiss, J. Phys. Chem. **92**, 4826 (1988).
[14] P. Nielaba, V. Privman, and J. S. Wang, J. Phys. A **23**, L1187 (1990); Phys. Rev. B **43**, 3366 (1991).
[15] J. D. Sherwood, J. Phys. A **23**, 2827 (1990).
[16] S. S. Manna and N. M. Švrakić, J. Phys. A **24**, L671 (1991).
[17] Lj. Budinski-Petković and U. Kozmidis-Luburić, Physica A **236**, 211 (1997).
[18] M. C. Bartelt and V. Privman, J. Chem. Phys. **93**, 6820 (1990).
[19] G. J. Rodgers, Phys. Rev. E **48**, 4271 (1993).
[20] S. Caser and H. J. Hilhorst, J. Phys. A **27**, 7969 (1994).